Boron-Doped Diamond Electrode Outperforms the State-of-the-Art Electrochemiluminescence from Microbeads Immunoassay

Boron-doped Diamond Electrode Outperforms the State-of-the-art Electrochemiluminescence from Microbeads Immunoassay

Kohei Sakanoue,[‡] Andrea Fiorani,*[‡] Claudio Ignazio Santo,[†] Irkham,[‡,#] Giovanni Valenti,[†] Francesco Paolucci[†] and Yasuaki Einaga*[‡]

Email: andrea.fiorani@keio.jp; einaga@chem.keio.ac.jp

[‡]Department of Chemistry, Keio University, 3−14−1 Hiyoshi, Yokohama 223−8522, Japan

[†]Department of Chemistry "G. Ciamician", University of Bologna, Via Selmi 2, 40126, Bologna, Italy

[#]Present address: Department of Chemistry, Padjadjaran University, Jalan Raya Bandung Sumedang Km. 21, Sumedang 45363, Indonesia

KEYWORDS: Immunosensor •Electrochemiluminescence • Boron-doped diamond • Ru(bpy)$_3^{2+}$ • tri-n-propylamine •Microbeads

ABSTRACT: Electrochemiluminescence (ECL) is a powerful transduction technique where light emission from a molecular species is triggered by an electrochemical reaction. Application to biosensors led to a wide range of electroanalytical methods with particular impact in clinical analysis for diagnostic and therapeutic monitoring. Therefore, the quest for increasing the sensitivity while maintaining reproducible and easy procedures as brought investigations and innovations in i) electrode materials, ii) luminophore and iii) reagents. Particularly, the ECL signal is strongly affected by the electrode material and its surface modification during the ECL experiments. Here, we exploit boron-doped diamond (BDD) as electrode material in microbeads-based ECL immunoassay to be compared with the approach used in commercial instrumentations. We conducted a careful characterization of ECL signals from tris(2,2'-bipyridine)ruthenium(II) (Ru(bpy)$_3^{2+}$)/tri-*n*-propylamine (TPrA) system, both in homogeneous (i.e., free diffusing Ru(bpy)$_3^{2+}$) and heterogeneous (i.e., Ru(bpy)$_3^{2+}$ bound on microbeads). We investigated the methods to promote TPrA oxidation, which led to the enhancement of ECL intensity, and the results revealed that the BDD surface properties greatly affect the ECL emission, so it does the addition of neutral, cationic or anionic surfactants. Our results from homogeneous and heterogeneous microbead-based ECL show opposite outcomes, which have practical consequence in ECL optimization. In conclusion, by using Ru(bpy)$_3^{2+}$-labelled immunoglobulins bound on microbeads, the ECL resulted in an increase of 70% and a double signal-to-noise ratio compared to platinum electrode which is actually used in commercial instrumentations for clinical analysis. This research infers that microbead-based ECL immunoassays with a higher sensitivity can be realized by BDD.

INTRODUCTION

The accurate and reproducible quantification of small molecules and biomolecules is nowadays spread through our society, with applications in food control, environmental analysis and medicine.[1] Among these, electrochemical methods account for a wide range of sensing technologies,[2] and beside the most famous glucose biosensor,[3] a wealth of electrochemical sensors face a daily use.[4,5] These technologies rely on different electrochemical techniques,[6] and in particular, electrochemiluminescence (ECL) is prominent in clinical diagnostic and therapeutic monitoring.[7-9]

ECL is a technique where an electrochemical reaction induces a light emission from a luminophore as a consequence of a high energetic electron transfer.[10-12] The electrochemical input combined with the light output give ECL unique features, such as very low background signal, a broad dynamic range, rapid measurements in small volumes, combined with spatial and temporal resolution of light emission.[13] In particular, the spatiotemporal resolution permits to perform ECL imaging on cells,[14] single entities[15-17] and to investigate reaction mechanisms.[18-20]

The efforts to increase the ECL emission, to achieve lower limit of detection (LOD), are focused on (i) the electrode material,[21] (ii) the coreactant,[22] and (iii) the luminophore.[23,24] In particular, recent examples of a new coreactant[18] and iridium complexes[25] have shown how ECL can benefit from these two approaches.

Electrode materials do not see an equal effort in the quest for an increased ECL emission, however ECL is primarily triggered by an electrochemical reaction where the electrode material plays a crucial role.[21,26] Carbonaceous material and noble metals are until now the materials of choice, distinguished by the dichotomy between high emission and long-term stability.[27-29] Carbon-based materials have the advantage of a high current for coreactant oxidation, but poor cycling

stability, making them suitable for disposable applications.[30] On the other hand, metal electrodes offer the advantage of continuous use,[31,32] but suffering from low emission due to surface oxide which hinders the coreactant oxidation.[21]
In these two previous examples, the coreactant is the tri-*n*-propylamine (TPrA),[33] which in combination with tris(2,2'-bipyridine)ruthenium(II) ($Ru(bpy)_3^{2+}$) is the only ECL system found in commercial applications, nowadays available in the market of clinical diagnostic.[30,31] Other coreactants, even if they have been discovered previously than TPrA,[34,35] didn't reach such a breakthrough.[7] This is ascribed to the favorable combination of energetic and mechanistic reactions involved in ECL immunoassay with $Ru(bpy)_3^{2+}$ and TPrA.[36]
For these reasons, an ideal electrode material should be stable for extended utilization, while retaining a good kinetics for the TPrA oxidation.
Boron-doped diamond (BDD) emerged as a new material for ECL,[37] and we recently demonstrated that BDD reaches a far superior emission than glassy carbon or platinum electrodes for the $Ru(bpy)_3^{2+}$/persulfate system.[38] Compared to carbon or metal electrodes, BDD has a wider potential window, low capacitive current and high chemical and physical stability[39] which enabled to uncover new ECL systems.[40,41] While some researches have been conducted[42-45] and also our group has been dedicated to apply BDD for ECL,[38,40,41,46,47] a thoughtful investigation of the $Ru(bpy)_3^{2+}$/TPrA system at BDD is still missing.
Here, we present a careful characterization of the ECL at BDD electrode addressing the question of TPrA oxidation and the means to enhance it. Furthermore, we investigated the BDD ability to generate the ECL from magnetic beads labelled with ruthenium complexes-antibody conjugate, which mimics exactly bead-based immunoassays, to reach finally an outstanding ECL emission that outperforms the current state-of-the-art system.

EXPERIMENTAL SECTION

Materials. Tris(2,2'-bipyridyl)ruthenium(II) chloride hexahydrate ($Ru(bpy)_3Cl_2 \cdot 6H_2O$, > 98.0%) and trimethyl borate ($B(OCH_3)_3$, > 98.0%) from Tokyo Chemical Industry (Tokyo, Japan). Potassium dihydrogen phosphate (KH_2PO_4, ≥ 99.5%), dipotassium hydrogen phosphate (K_2HPO_4, ≥ 99.0%), phosphoric acid (H_3PO_4, ≥ 85.0%), sodium perchlorate monohydrate ($NaClO_4 \cdot H_2O$, ≥ 98.0%) and dimethyl-sulfoxide (DMSO, Super dehydrated, ≥ 99.0%) from Wako (Osaka, Japan). Tri-*n*-propylamine (TPrA, $(CH_3CH_2CH_2)_3N$, ≥ 98.0%), sodium dodecyl sulfate (SDS, $CH_3(CH_2)_{11}OSO_3Na$, ≥ 99.0%), nonaethylene glycol monododecyl ether ($C_{12}E_9$, $HO(CH_2CH_2O)_9(CH_2)_{11}CH_3$), trimethyl-tetradecylammonium chloride (TTAC, $CH_3(CH2)_{13}N(CH_3)_3Cl$, ≥ 98.0%), biotinamidohexanoic acid N-hydroxysuccinimide ester (≥ 98%), N,N'-dicyclohexylcarbodiimide (DCC, ≥ 99.0%), N-hydroxysuccinimide (NHS, 98%) and TWEEN® 20 from Sigma-Aldrich (St. Louis, MO). Acetone (CH_3COCH_3, ≥ 99.5%) and N,N-dimethylformamide (DMF, ≥ 99.5%) from Kanto Chemical (Tokyo, Japan). ChromPure Mouse IgG, whole molecule (IgG, Code: 015-000-003, 5.7mg/mL) from Jackson Immuno Research (West Grove, PA). Bis(2,2'-bipyridine)-[4-(4'-methyl-2,2'-bipyridin-4-yl)butanoic acid] ruthenium bis(hexafluorophosphate) from Cyanagen (Bologna, Italy). Paramagnetic microbeads Dynabeads™ M-280 Streptavidin (diameter 2.8 μm, 10 mg/mL) from Thermo Fisher Scientific (Waltham, MA). Spectra-Por® Float-A-Lyzer® G2 from REPLIGEN (Waltham, MA) Filters for dialysis. Doubly distilled water with a maximum conductivity of 18.2 MΩ•cm was provided by a Simply–Lab water system (DIRECT-Q UV3, Millipore, Burlington, MA). All reagents were used without further purification. Throughout the experiments phosphate buffer (PB) 0.2 M is used, except otherwise stated.
Preparation of the BDD Electrodes. BDD films were deposited on silicon (111) wafers (Shinwa Tsusho, Japan) using a microwave plasma-assisted chemical vapor deposition (MPCVD) system (CORNES Technologies/ASTeX-5400). Acetone and trimethyl borate were used as the carbon and boron sources, respectively, with an atomic ratio of B/C 1% ([B] in BDD ≈ 2×10^{21} cm^{-3}). Raman spectra were recorded with an Acton SP2500 (Princeton Instruments) with excitation wavelength of 532 nm from a green laser diode at ambient temperature, while the surface morphology of the BDD was examined with a field emission scanning electron microscope (SEM, JCM-6000, JEOL, Japan) (Figure S1). Also, the boron concentration in the BDD electrode was measured by glow discharge optical emission spectrometry (GD-OES, GD-Profiler2, Horiba Ltd., Japan) (Figure S1).
Electrochemistry. Electrochemical measurements were conducted with a potentiostat PGSTAT302N (Metrohm). Electrochemical impedance spectroscopy (EIS) was conducted by ModuLab XM ECS (Solartron Analytical, Farnborough, U.K.) with an amplitude of 10 mV in the frequency range from 1 MHz to 100 mHz. The PTFE cell is a single-compartment with 1% BDD as the working electrode (geometric area 0.75 cm^2), a Pt spiral as the counter electrode, and an Ag/AgCl (saturated KCl) electrode as the reference electrode. EIS measurements were based on a previously established procedure,[46] the geometric area for the working electrode was 0.072 cm^2. For ECL with paramagnetic microbeads a different arrangement was used: the working electrode geometric area was 0.28 cm^2 for 1% BDD or Pt, counter was a Pt disk electrode (0.072 cm^2) and reference was an Ag/AgCl (3 M NaCl) electrode. Generally, Ag/AgCl (saturated KCl) has been used for measurements in homogeneous solution ($Ru(bpy)_3^{2+}$ and TPrA free to diffuse), while Ag/AgCl (3 M NaCl) in heterogeneous assay ($Ru(bpy)_3^{2+}$ bound on microbeads). For clarity, the type of reference electrode is reported when needed, otherwise potential scale conversion has been used.[48]
ECL. The ECL signals were measured with a photomultiplier tube (PMT, Hamamatsu R928) placed at a fixed height from the electrochemical cell. Both the electrochemical cell and the PMT were contained inside a dark box. A high-voltage power

socket assembly with a transimpedance amplifier (Hamamatsu C6271) was used to supply 500 V to the PMT, using an external trigger connection to the potentiostat DAC module. Light/current/voltage curves were recorded by collecting the amplified PMT output signal with the ADC module of the potentiostat. ECL spectra were collected by a SEC2000 Spectra system UV-visible spectrophotometer (ALS Co. Ltd., Japan). For all ECL experiments, error bar shows the standard deviation (n = 3).

ECL imaging. This instrumentation was described in detail previously.[18] Briefly, the PTFE homemade electrochemical cell comprises a 1% BDD working electrode (geometric area 3.5 cm^2), Pt wire counter electrode, and Ag/AgCl (3 M KCl) reference electrode. ECL images acquisition is based on an epifluorescence microscope from Nikon (Chiyoda, Tokyo, Japan) coupled with an ultrasensitive EM-CCD camera (EM-CCD 9100-13 from Hamamatsu, Hamamatsu, Japan) with long-distance objectives from Nikon (20 × /0.40 DL13 mm). The EM-CCD camera signal acquisition (integration time 8 s) was triggered with by a potentiostat. Electrochemical cell and microscope were enclosed in a dark box to avoid interferences from external light. For all ECL imaging experiments, error bar shows the standard deviation (n = 3).

Working electrodes pretreatment and cleaning. Prior to each measurement, the BDD surface was pretreated to guarantee reproducibility: i) cathodic reduction at −3.5 V followed by anodic oxidation at +3.5 V (hereinafter, called AO-BDD), or ii) anodic oxidation at +3.5 V followed by cathodic reduction at −3.5 V (hereinafter, called CR-BDD), in 0.1 M $NaClO_4$ solution for a total fixed charge of 0.15 C cm^{-2} in each step (Figure S2a). Pt foil (Nilaco Co., Japan) electrode was cleaned with a 0.5 μm alumina suspension on cloth tape, then sonicated in double-distilled water for 2 min (2 times), and dried with a nitrogen stream. Furthermore, the Pt electrode was cycled in 0.2 M PB (pH 7) between 1.0 V and −0.7 V to assure a clean and reproducible electrode surface (Figure S2b).

Conjugation of ruthenium ECL labels with the immunoglobulin and ECL assay. A detailed procedure, adapted from previous reports[25,49,50] is available in the Supporting Information (Scheme S1-S3 and Figure S3, S4). Firstly, IgG was reacted with biotin to make **IgG-biotin**. Secondly, bis(2,2'-bipyridine)-[4-(4'-methyl-2,2'-bipyridin-4-yl)butanoic acid] ruthenium(II) was activated with EDC/NHS and reacted with **IgG-biotin** to obtain **Ru-IgG-biotin**. Finally, **Ru-IgG-biotin** conjugate was loaded on streptavidin magnetic microbeads by biotin-streptavidin interaction to obtain **Ru@bead**. For the ECL measurements, **Ru@bead** were placed in the electrochemical cell and attracted on the working electrode by means of a magnet, then the TPrA solution was added and the ECL triggered by applying a suitable potential. For all ECL assays with beads, error bar shows the standard deviation (n = 3).

RESULTS AND DISCUSSION

Diamond, a material made entirely of sp^3 carbon, is a semiconductor with a very wide band gap (5.47 eV).[51] Similar to other semi-conductors, (i) doping gives diamond semi-metallic characteristic (above $\sim 10^{20}/cm^3$)[39] for unique applications in electrochemistry. Beside doping, the (ii) non-diamond carbon impurity (sp^2 carbon), (iii) crystal structure and (iv) surface termination affect the electrochemical behavior.

The doped diamond chosen for the present study is 1% boron in the boron/carbon source, since this percentage will assure a metal-like conductivity ([B]$\sim 10^{21}/cm^3$) without the side effect of introducing non-diamond carbon[46] (Figure S1). In fact, the actual boron concentration in the BDD electrode was 2.06 % ([B] = $3.62 \times 10^{21}/cm^3$) (Figure S1). The diamond structure is polycrystalline, albeit single crystals BDD are fabricated, they are suitable for particular applications (e.g., STM tips),[52] moreover the use in electrochemistry is also limited by the complexity to obtain large crystals on a millimeter scale.

Finally, the termination describes the functionalities bound to the terminal carbon on the surface of the diamond. From the MPCVD, owing to the reductive environment by hydrogen plasma, the surface is hydrogen terminated. However, oxygen termination can develop by air exposure or after electrochemical use, for a range of oxygen functional groups, such as hydroxyls, ethers, and carbonyl[53] or quinones.[54] Since the electrode materials and their surface state affect greatly the ECL response,[21] we may expect hydrogen and oxygen terminated BDD to exert this effect, as well.

We previously established that the surface of BDD can be modified by electrochemical pretreatment by applying anodic or cathodic currents which results in anodic oxidation (AO) and cathodic reduction (CR) BDDs, respectively.[55,56] The changes of surface termination will give two advantages: first, the surface properties can be tuned, and second, after the electrochemical measurement the surface can be restored to the initial state.

ECL at BDD. The effect of AO and CR on the ECL emission at BDD electrode is shown in Figure 1 by cyclic voltammetry (CV) measurements.

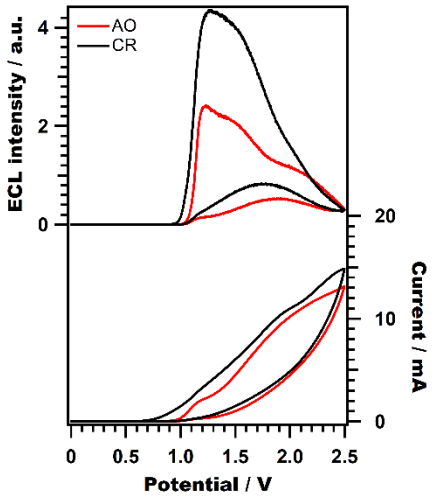

Figure 1. ECL intensity and cyclic voltammogram for 10 µM $Ru(bpy)_3^{2+}$ and 100 mM TPrA in 0.2 M PB (pH 8.0) on AO-BDD (red) and CR-BDD (black) electrodes. Scan rate: 100 mV s^{-1}.

The ECL shows two better results for CR-BDD compared to AO-BDD, higher intensity and lower onset potential[57] of emission. This result is a direct consequence of the difference in the kinetics of TPrA oxidation, where a higher current for CR-BDD leads to higher ECL intensity that is described by the oxidative-reduction mechanism[33] (Scheme 1).

Scheme 1. Oxidative-reduction ECL mechanism and corresponding physical-chemical parameters.[58] Potentials vs Ag/AgCl(KCl sat). P_1 is the degradation product of $TPrA^{\bullet}$ by oxidation and following hydrolysis.

$$TPrAH^+ \rightleftarrows TPrA + H^+ \qquad pKa = 10.4^{59} \quad (1)$$

$$TPrA \rightleftarrows TPrA^{\bullet+} + e^- \qquad E^0 = 0.92\ V^{59} \quad (2)$$

$$TPrA^{\bullet+} \rightleftarrows TPrA^{\bullet} + H^+ \qquad t_{1/2} = 0.7\ ms^{18} \quad (3)$$

$$Ru(bpy)_3^{2+} \longrightarrow Ru(bpy)_3^{3+} + e^- \qquad E^0 = 1.07\ V^{60} \quad (4)$$

$$Ru(bpy)_3^{3+} + TPrA^{\bullet} \longrightarrow Ru(bpy)_3^{2+*} + P_1 \qquad \Delta G = -0.54\ eV \quad (5)$$

$$Ru(bpy)_3^{2+*} \longrightarrow Ru(bpy)_3^{2+} + h\nu \qquad \lambda_{em} = 2.19\ eV^{60} \quad (6)$$

The lower onset potential for ECL emission depends on TPrA oxidation as well, although by a different mechanism which requires only TPrA oxidation[18,61,62] (eqs 1-3) and not the direct $Ru(bpy)_3^{2+}$ oxidation at the electrode (eqs 7-9), for an overall reaction mechanism as Scheme 2.

Scheme 2. Main mechanism involved in ECL emission before $Ru(bpy)_3^{2+}$ oxidation.[58] P_1 is the degradation product of $TPrA^{\bullet}$ by oxidation and following hydrolysis.

$$TPrAH^+ \rightleftarrows TPrA + H^+ \quad (1)$$

$$TPrA \rightleftarrows TPrA^{\bullet+} + e^- \quad (2)$$

$$TPrA^{\bullet+} \rightleftarrows TPrA^{\bullet} + H^+ \quad (3)$$

$$Ru(bpy)_3^{2+} + TPrA^{\bullet} \longrightarrow Ru(bpy)_3^{+} + P_1 \qquad \Delta G = -0.23\ eV \quad (7)$$

$$Ru(bpy)_3^{+} + TPrA^{\bullet+} \longrightarrow Ru(bpy)_3^{2+*} + TPrA \qquad \Delta G = -0.16\ eV \quad (8)$$

$$Ru(bpy)_3^{2+*} \longrightarrow Ru(bpy)_3^{2+} + h\nu \quad (9)$$

For this reason, it is highly affected by TPrA oxidation rate and we must recall Scheme 2 is the only active mechanism in ECL immunoassay (ruthenium complex is typically not free to diffuse, but bound on the immune complex) that highlights the importance to achieve a high TPrA oxidation rate. The ECL results observed on the two different BDD surfaces are ascribable to the higher content of hydrogen termination in CR-BDD compared to AO-BDD that is responsible for an increasing hydrophobicity of the electrode surface.[55,56,63] Facilitating the adsorption of the hydrophobic TPrA molecule on the electrode surface[28,64] leads to higher oxidation currents, and consequently an increased ECL intensity from contribution of the mechanism reported in Scheme 1, and lower potential onset from contribution of the mechanism reported in Scheme 2 before the oxidation potential of $Ru(bpy)_3^{2+}$. From ECL spectrum, it is clear that emission is only from $Ru(bpy)_3^{2+}$ excited state at 610 nm which is observed for all potentials range (Figure S5).

To confirm the role of TPrA oxidation, we measured the apparent heterogeneous rate constant of electron transfer (k_{ET}) for TPrA at the two electrode surfaces (Figure 2 and S6-S8). AO-BDD and CR-BDD gave values at 0.92 V (k^0_{ET}) of 0.0007 cm s^{-1} and 0.0075 cm s^{-1}, respectively. These results confirm that the large difference in current oxidation is the direct consequence of the rate of k_{ET} being one order of magnitude higher for CR-BDD compared to AO-BDD. For comparison, the value of k^0_{ET} for TPrA oxidation on glassy carbon is 0.6 cm s^{-1},[59] while on carbon nanotubes k_{ET} at 1.0 V is 0.026 cm s^{-1}.[65]

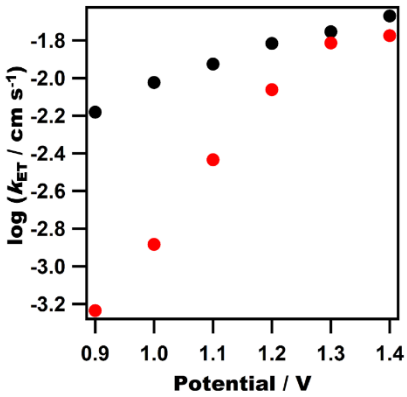

Figure 2. Logarithmic plot of k_{ET} for TPrA oxidation at AO-BDD (red) and CR-BDD (black) as function of the applied potential.

The effect of TPrA oxidation rate is limited in the lower potential range as the values of k_{ET} tend to converge from 1.3 V, however this difference is substantial to leads in a twofold increase of the ECL emission. Because CR-BDD showed better performance than AO-BDD, this surface termination was selected for the following experiments on the $Ru(bpy)_3^{2+}$/TPrA system.
As can be seen from Scheme 1 and Scheme 2, pH of electrolyte (i.e., TPrA acid-base equilibrium) and TPrA concentration are of fundamental importance, therefore, these two parameters have been optimized to maximize the ECL emission (Figure 3 and S9-S10).

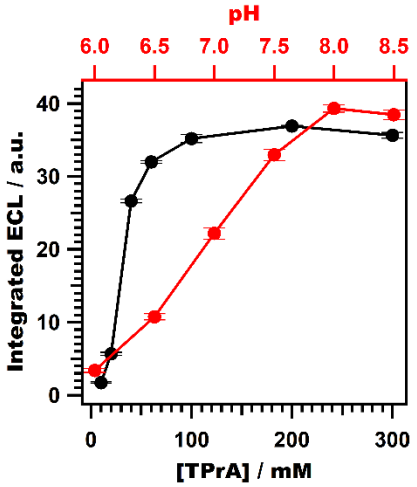

Figure 3. Optimization of pH with 100 mM TPrA (red) and TPrA concentration at pH 8 (black) with 10 µM $Ru(bpy)_3^{2+}$ in 0.2 M PB.

The ECL emission increased up to 100 mM TPrA, while above this concentration the value is stable and limited by the $Ru(bpy)_3^{2+}$ availability. Concerning the pH, an increase shifts the acid-base equilibrium of TPrA (pKa = 10.4) from the protonated to neutral form that is the electroactive species leading to ECL increase.[33,59] From these two optimizations, we opted for 100 mM TPrA and pH 8 for the following investigations.
Additionally, the stability of ECL generation on BDD was investigated and compared with that on Pt (Figure S11). As a result, we confirmed that BDD can provide more stable ECL emission than Pt can.
Surfactant addition. For the $Ru(bpy)_3^{2+}$/TPrA system, what makes ECL emission to increase, it is the ability by the electrode to promote TPrA oxidation reaching high currents, as we demonstrated for AO-BDD and CR-BDD.
In case of noble metal (e.g., Au, Pt) electrodes, an effective method to accelerate the TPrA oxidation rate is the addition of surfactants in solution which adsorb on the electrode surface and increase its hydrophobicity.[21,28,64] At the same time, surfactants reduce the development of hydrophilic surface oxide layers which hinder the heterogeneous electron transfer. We investigated if surfactants can exert a similar effect at BDD electrode. However, there is little knowledge about surfactants at BDD electrodes, therefore we chose three different surfactants, namely trimethyl-tetradecylammonium chloride (TTAC), sodium dodecyl sulfate (SDS), and nonaethylene glycol monododecyl ether ($C_{12}E_9$) which carry positive,

negative, and no charge, respectively. The ECL response was evaluated for a range of surfactant concentrations near the critical micelle concentration (CMC), as this parameter shows sharp response of the surfactant effects on the system under investigation[66,67] (Figure 4 and S12).

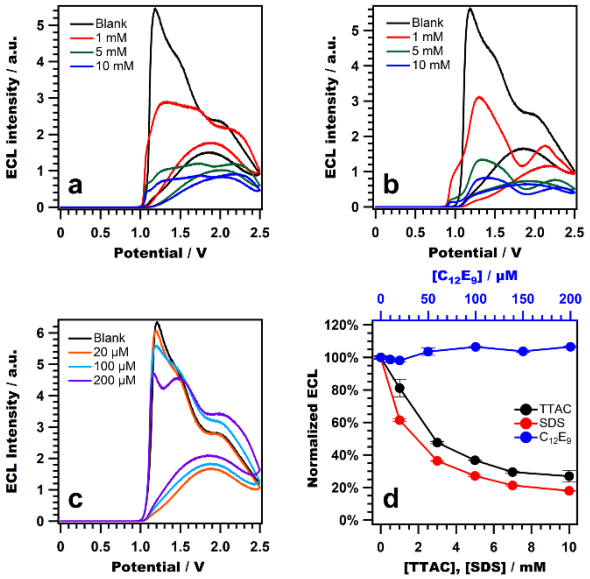

Figure 4. CV-ECL response for the addition of surfactants in solution: a) TTAC (4.5 mM), b) SDS (8.2 mM), and c) $C_{12}E_9$ (83 µM); concentrations in parenthesis are CMC in water.[68] Solution: 10 µM $Ru(bpy)_3^{2+}$ and 100 mM TPrA in 0.2 M PB (pH 8.0) at CR-BDD. Panel d) shows the integral of ECL intensity as function of surfactant concentration.

From the results in Figure 4, it is clear that for TTAC and SDS the ECL emission was severely affected with a decrease of 74 and 82%, respectively. The ECL was stable for $C_{12}E_9$ addition, however it decreased in the range 1-1.5 V and increased in the range 2-2.5 V. Unfortunately, for the three surfactants investigated, the enhancement sought did not occur suggesting that in the case of BDD electrode, the addition of surfactant resembles the behavior of glassy carbon, which ECL is also affected negatively by surfactants.[64,69,70] However, focusing on the ECL emission in the case of SDS, the region below 1.0 V showed a new peak. This effect of SDS might be related to the electric charge of the head group because a negatively charged molecule can adsorb more easily on hydrogen terminated BDD surface, which is slightly positive charged.[39]
To investigate the ECL emission behind this peak, a range of SDS concentrations was measured by chronoamperometry at 0.95 V (Figure 5), which is the peak potential observed in the CV-ECL intensity profile of Figure 4b.

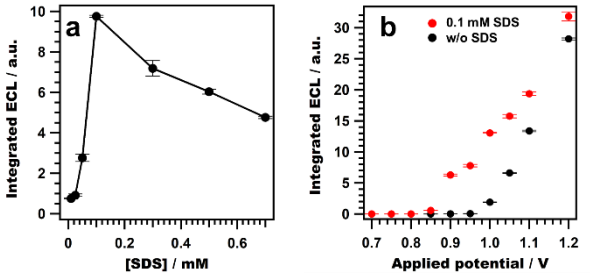

Figure 5. Integrated ECL as function of SDS concentration (a). Integrated ECL as function of the applied potential with 0.1 mM SDS (b). Solution: 10 µM $Ru(bpy)_3^{2+}$ and 100 mM TPrA in 0.2 M PB (pH 8.0) on CR-BDD.

In this case, a positive effect of SDS addition was verified by an ECL emission increase up to 0.1 mM of SDS. The chronoamperometry profiles of the ECL intensity showed a sharp increase with enhanced ECL intensity (Figure S13a) that indicated a promotion of TPrA oxidation in terms of faster reaction rate. The beneficial role of SDS was also confirmed as function of the potential (Figure 5b) with a remarkable increase of ECL at potentials below $Ru(bpy)_3^{2+}$ oxidation (i.e., 0.90-0.95 V) where only TPrA oxidation is involved in the ECL generation as depicted in Scheme 2. Possible oxidation processes upon SDS (Figure S13c) and effects on potential shift of $Ru(bpy)_3^{2+}$ oxidation by the addition of SDS (Figure S13) have been excluded. Taking into account this result, SDS should also enhance the ECL emission in heterogeneous immunoassay systems, that is, where $Ru(bpy)_3^{2+}$ is immobilized on the immunocomplex at a distance preventing its direct oxidation at the electrode, and TPrA oxidation is the only relevant factor that initiates the light emitting process. Beyond 0.1 mM, the ECL

intensity showed a decrease with SDS addition, while the oxidation current leveled at stable values (Figure S13b). Because the oxidation current was not affected by SDS concentration above 0.1 mM, we might infer this ECL decrement is associated to homogeneous quenching in solution of the $Ru(bpy)_3^{2+}$ excited states. This hypothesis is supported and in agreement with a previous report on SDS effects on ECL[69] and $Os(bpy)_3^{2+}$ excited stated quenching.[71] In conclusion, we can ascribe this trend of the ECL emission to two opposite effects induced by SDS addition, i) adsorption on the BDD with increasing hydrophobic surface and consequently higher TPrA oxidation rate, and ii) quenching of $Ru(bpy)_3^{2+}$ excited states. To be thorough, we investigated also the effect of halide ions (i.e., chloride, bromide, and iodine) which have been proposed to enhance the ECL emission,[28] although this effect was not observed for BDD electrodes (Figure S15).

ECL Immunoassay. With the promising results of CR-BDD and SDS addition, we tested the efficacy on a real setting to prove the usefulness of BDD in ECL analysis. Generally, ECL sandwich immunoassay involves the capture of antibody-antigen complex either directly on electrodes or on polystyrene beads with a magnetic core (Figure S16).[7,25] BDD adapts better for bead-based immunoassay, as the sp^3 carbon structure is slightly suitable for bioconjucation, therefore, as a proof of concept, we investigated the ECL from magnetic polystyrene beads decorated with an antibody-labelled ruthenium complex (**Ru@bead**) that mimics exactly an ECL immunoassay.

The ECL emission by ECL imaging and CV from a single **Ru@bead** on BDD electrode are shown in Figure 6. In addition, ECL imaging is also useful to prove that the ruthenium complex is bound on the beads and not free to diffuse in solution (Figure S17), as we confirmed from absence of ECL from the supernatant of beads washing solution after ruthenium complex loading (Figure S4) which proves we were mimicking exactly an ECL immunoassay. According to the mechanism of Miao et al.,[61] with reexamination by Zanut et al.,[Errore. Il segnalibro non è definito.18] the emission is described by Scheme 2. Only this mechanism is available for ECL generation when the ruthenium complex cannot be oxidized at the electrode directly, and it is highly dependent on TPrA oxidation rate. For this reason, we examined again both CR-BDD and AO-BDD electrodes as changes in the mechanisms can brought a possible paradigm shift in the results. As a matter of fact, with a **Ru@bead** the higher ECL was registered by AO-BDD instead of CR-BDD, in contrast to homogeneous case, where $Ru(bpy)_3^{2+}$ is free to diffuse in solution (Figure 6c-d). The CV measurements on single **Ru@bead** confirmed the higher emission for AO-BDD and the emission potential beyond 1.0 V is the direct consequence of the dependence on TPrA oxidation rate as the only mechanism active in ECL generation (Figure 6e and S17).

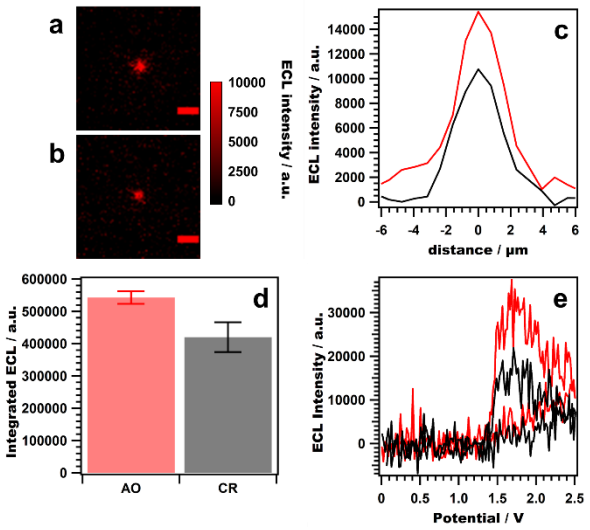

Figure 6. ECL imaging from 2.8 µm **Ru@bead** for AO-BDD (a) and CR-BDD (b). The images were obtained by applying a constant potential of 1.7 V for 4 s. Scale bar: 10 µm. Comparison of the bead profile lines (c) and integrated ECL (d) for AO-BDD (red) and CR-BDD (black). ECL intensity by CV obtained from single **Ru@bead** (e) at 100 mV s^{-1} (integration time xyz ms). Solution: 100 mM TPrA in 0.2 M PB (pH 7.0).

To confirm the result of ECL imaging on single bead, the ECL emission from multiple **Ru@bead** was also investigated which provides a more accurate representation of the commercial immunoassay system (Figure 7). The collective **Ru@bead** provided a similar ECL emission behavior to that from a single bead where AO-BDD was superior to CR-BDD in generating ECL. Noteworthy that the negative shift of the ECL onset potential for CR-BDD compared to AO-BDD, still suggesting a faster TPrA oxidation rate at low potentials, confirmed by higher current values (Figure S18).

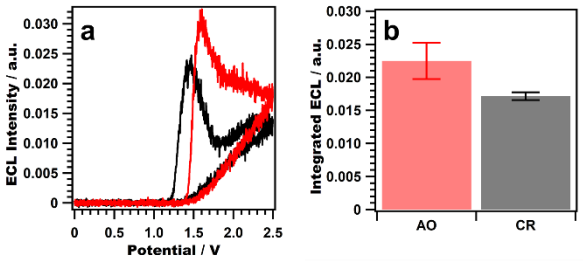

Figure 7. ECL intensity by CV (a) and integrated ECL (b) obtained from **Ru@bead**: multibeads detection by PMT. Solution: 100 mM TPrA in 0.2 M PB (pH 7.0) on CR-BDD (black) and AO-BDD (red).

The effect of SDS addition to the $Ru(bpy)_3^{2+}$/TPrA system showed a promotion of TPrA oxidation, which led to enhanced ECL emission. However, in the heterogeneous ECL system with **Ru@bead** this effect was not attained, for both AO-BDD and CR-BDD (Figure S19).
Albeit lower SDS concentration were used compared to the homogenous case, the presence of a protein layer on the magnetic beads might be responsible for SDS adsorption[72,73] and $Ru(bpy)_3^{2+}$ excited state quenching.
Further investigation of the measurement conditions for BDD by using **Ru@bead** resulted in the optimal pH of 7 (Figure S20) and 100 mM TPrA (Figure S21).
ECL relationship with pH is dictated by two opposite effects: i) pH increase will bring a higher amount of free TPrA available for oxidation (i.e., $TPrAH^+$ is not electroactive, pKa = 10.4) leading to higher ECL, as higher concentrations of free TPrA can be observed by the increment of anodic current with pH (Figure S20b) meanwhile, ii) higher concentration of hydroxyl ions promote the $TPrA^{\bullet+}$ deprotonation by protons scavenging which leads to lower ECL (Figure S20c). The $TPrA^{\bullet+}$ deprotonation (eq. 3) can be considered as a pseudo first-order reaction in the proton concentration,[74] and it is also affected by the buffer capacity.[75] Concerning the TPrA concentration (Figure S21), obviously an increase generates higher ECL, while the decrease can be correlated to the reductive quenching[76] of $Ru(bpy)_3^{2+}$ excited stated by TPrA in an electron transfer reaction similarly to other tertiary amines that can quench the excited state of ruthenium complexes by electron transfer.[77]
Finally, optimization of the applied potential which generated the higher ECL signal resulted in 2.4 V for AO-BDD and 1.6 for CR-BDD (Figure S22).
Opposing results from free diffusing $Ru(bpy)_3^{2+}$ in solution and in the heterogeneous case (i.e., bound on magnetic beads) bring out the relative efficiency of the ECL mechanisms. In our case, the gap in k_{ET} for TPrA oxidation tends to fade away from 1.3 V (Figure 2) and the current values for TPrA oxidation are similar from 1.4 V, slightly higher for CR-BDD (Figure S23), therefore, the amount of oxidized TPrA cannot account for the lower ECL emission of CR-BDD. In addition, we can exclude that ECL is generated from background emission (Figure S22). It has been reported that the surface state is responsible for large variation of ECL by maintaining a similar current value for TPrA oxidation,[78] and this might be responsible for this contrasting result on the different surface state of BDD. With all the experimental parameters optimized, the ECL at BDD had to be benchmarked to assess the full potential in analytical applications. ECL efficiency is usually a parameter used to compare different ECL systems with $Ru(bpy)_3^{2+}$ as the reference luminophore.[8,10] However, reporting the ECL efficiency has recently been questioned with recommendations for measurement methods.[79,80] Likely, the ECL efficiency is affected by $Ru(bpy)_3^{2+}$ and TPrA ratio,[80] as different mechanisms take part,[59] and we might expect an effect by electrode material, as well. To obtain a useful information of ECL from **Ru@bead** at BDD, we compared the emission with Pt electrode which is used in analytical instrumentations with beads conjugates for clinical analysis,[9,32] therefore holding a technological interest. Moreover, the parameters for ECL are already optimized[18,81,82] making the comparison straightforward. We only optimized the potential for the utilization in our homemade electrochemical cell to take into account the effect of ohmic drop on the applied potential (Figure S24).
As shown in Figure 8, AO-BDD has a superior ability to produce ECL as the emission reached a value 70% higher than Pt (Figure S25). Metal electrodes, such as Pt, are known to develop a layer of metal oxide during potential application that suppresses the ECL signal by hindering TPrA oxidation. For this reason, they benefit from addition of surfactants to prevent the formation of the surface oxides and enhance the ECL signal.[21,28,64,70,83] However, BDD can reach a higher ECL signal without surfactant addition, which has been used for Pt in the present case (i.e., $C_{12}E_9$),[18] it shows a signal-to-noise ratio for AO-BDD that is 2 times higher than Pt (Figure S22 and S24), and noteworthy, by using BDD the amount of TPrA needed was lowered from 180 mM to 100 mM with a significant savings of this toxic[84] and relatively expensive chemical. For the sake of comparison, we included the ECL from **Ru@bead** at glassy carbon electrode (Figure S26). However, carbon electrodes are not suited for long-time application as they best fit disposable device.[30,85]

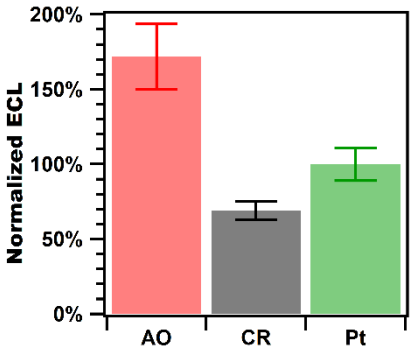

Figure 8. Integrated ECL of Ru@bead obtained by chronoamperometry for AO-BDD at 2.4 V (red), CR-BDD at 1.6 V (black), and Pt at 1.5 V (green). Solutions: 100 mM TPrA in 0.2 M PB (pH 7) for both AO-BDD and CR-BDD electrodes; 180 mM TPrA and 0.1wt% C12E9 surfactant in 0.2 M PB (pH 6.9) for Pt electrode.

Based on the superior ECL emission compared to Pt and the stability of ECL signal, we can infer that BDD could be suited for long-term application while providing higher sensitivity in ECL immunoassay, in particular for analyzers based on flow cell systems.[32]
BDD electrodes are finding their way toward electroanalytical applications,[86] and these results can be a step forward for its practical application beyond fundamental studies to expand the frontiers of ECL immunoassays and BDD electrodes.

CONCLUSION

Here, we investigated the ECL behavior on BDD electrode for the $Ru(bpy)_3^{2+}$/TPrA system. The effect of BDD surface, namely oxygen terminated and hydrogen terminated, resulted in large variation of the ECL signal with the best result for hydrogen terminated BDD, when $Ru(bpy)_3^{2+}$ is free to diffuse in solution, according to a higher electron transfer constant for TPrA oxidation promoted by BDD surface hydrophobicity. The BDD surface properties have a major contribution in the TPrA oxidation, consequently the addition of several surfactants was investigated as an approach to enhance the TPrA oxidation on BDD, albeit this approach did not result in a clear ECL enhancement, sodium dodecyl sulfate can be beneficial under μM concentration when $Ru(bpy)_3^{2+}$ is in solution. The ability of BDD to generate ECL from ruthenium-labelled beads, which resembles the ECL immunoassay system for clinical analysis, showed the best results from oxygen terminated surface, in opposition to free $Ru(bpy)_3^{2+}$. With the optimized conditions for the ECL signal, namely surface termination, TPrA concentration and pH, the BDD electrode was able to generate a 70% higher ECL intensity and a double signal-to-noise ratio than Pt, which is actually the standard electrode in ECL immunoassay analyzer used in clinical diagnostic. This result suggests that more sensitive ECL immunoassay could be developed by using BDD electrode.

ASSOCIATED CONTENT

Supporting Information. Electrochemical and ECL data of boron-doped diamond; procedure of immunoglobulin G conjugation with ruthenium complex and loading on magnetic beads; ECL imaging of beads; ECL parameters and surfactants optimization; ECL comparison with Pt electrode. This material is available free of charge via the Internet at http://pubs.acs.org.

AUTHOR INFORMATION

Corresponding Author

*andrea.fiorani@keio.jp
*einaga@chem.keio.ac.jp

Author Contributions

The manuscript was written through contributions of all authors. All authors have given approval to the final version of the manuscript.

ACKNOWLEDGMENT

A.F. acknowledges the Japan Society for the Promotion of Science (Fellowship ID No. P19333) and Grant-in-Aid for JSPS Fellows (Grant 19F19333). Furthermore, this work was partially supported by JSPS Grant-in-Aid for Scientific Research A 19H00832 (to Y E.).

ABBREVIATIONS

BDD, boron-doped diamond; TPrA, tri-*n*-propylamine; $Ru(bpy)_3^{2+}$, tris(2,2'-bipyridine)ruthenium (II); AO-BDD, anodic oxidation boron-doped diamond; CR-BDD, cathodic reduction boron-doped diamond; P_1, the degradation product of $TPrA^{\bullet}$ by oxidation and following hydrolysis; Ru@bead, bead labelled with tris(2,2'-bipyridine)ruthenium (II) complexes.

REFERENCES

([1]) Luong, J. H. T.; Male, K. B.; Glennon, J. D. Biosensor technology: Technology push versus market pull. *Biotechnol. Adv.* **2008**, *26* (5), 492-500.

([2]) Ronkainen, N. J.; Halsall, H. B.; Heineman, W. R. Electro-chemical biosensors. *Chem. Soc. Rev.* **2010**, 39 (5), 1747-1763.

([3]) Wang, J. Electrochemical Glucose Biosensors. *Chem. Rev.* **2008**, *108* (2), 814-825.

([4]) Turner, A. P. F. Biosensors: sense and sensibility. *Chem. Soc. Rev.* **2013**, *42* (8), 3184-3196.

([5]) Pereira da Silva Neves, M. M.; González-García, M. B.; Hernández-Santos, D.; Fanjul-Bolado, P. Future trends in the market for electrochemical biosensing. *Curr. Opin. Electrochem.* **2018**, *10*, 107-111.

([6]) Grieshaber, D.; MacKenzie, R.; Janos Vörös, J.; Reimhult, E. Electrochemical Biosensors - Sensor Principles and Architectures. *Sensors* **2008**, *8* (3), 1400-1458

([7]) *Analytical Electrogenerated Chemiluminescence: From Fundamentals to Bioassays*; Sojic, N., Ed.; Detection Science Series No. 15; The Royal Society of Chemistry: London, **2020**.

([8]) Miao, W. Electrogenerated Chemiluminescence and Its Biorelated Applications. *Chem. Rev.* **2008**, *108* (7), 2506-2553

([9]) Imai, K.; Watari, S.; Sakazume, T.; Mitsuyama, S. Clinical Chemistry and Immunoassay Testing Supporting the Individual Healthy Life. *Hitachi Rev.* **2008**, *57*, 1-7.

([10]) Richter, M. M. Electrochemiluminescence (ECL). *Chem. Rev.* **2004**, *104* (6), 3003–3036.

([11]) Hesari, M.; Ding, Z. Review-Electrogenerated Chemiluminescence: Light Years Ahead. *J. Electrochem. Soc.* **2016**, *163* (4), H3116-H3131.

([12]) Fiorani, A.; Valenti, G.; Iurlo, M.; Marcaccio, M.; Paolucci, F. Electrogenerated chemiluminescence: A molecular electrochemistry point of view. *Curr. Opin. Electrochem.* **2018**, *8*, 31-38.

([13]) Zanut, A.; Fiorani, A.; Rebeccani, S.; Kesarkar, S.; Valenti, G. Electrochemiluminescence as emerging microscopy techniques. *Anal. Bioanal. Chem.* **2019**, *411* (19), 4375-4382.

(14) Valenti, G.; Scarabino, S.; Goudeau, B.; Lesch, A.; Jović, M.; Villani, E.; Sentic, M.; Rapino, S.; Arbault, S.; Paolucci, F.; Sojic, N. Single Cell Electrochemiluminescence Imaging: From the Proof-of-Concept to Disposable Device-Based Analysis. *J. Am. Chem. Soc.* **2017**, *139* (46), 16830-16837.

(15) Ma, Y.; Colin, C.; Descamps, J.; Arbault, S.; Sojic, N. Shadow Electrochemiluminescence Microscopy of Single Mitochondria. *Angew. Chem. Int. Ed.* **2021**, *60* (34), 18742-18749.

(16) Liu, Y.; Zhang, H.; Li, B.; Liu, J.; Jiang, D.; Liu, B.; Sojic, N. Single Biomolecule Imaging by Electrochemiluminescence. *J. Am. Chem. Soc.* **2021**, *143* (43), 17910-17914.

(17) Pan, S.; Liu, J.; Hill, C. M. Observation of Local Redox Events at Individual Au Nanoparticles Using Electrogenerated Chemiluminescence Microscopy. *J. Phys. Chem. C* **2015**, *119* (48), 27095-27103.

(18) Zanut, A.; Fiorani, A.; Canola, S.; Saito, T.; Ziebart, N.; Rapino, S.; Rebeccani, S.; Barbon, A.; Irie, T.; Josel, H.-P.; Negri, F.; Marcaccio, M.; Windfuhr, M.; Imai, K.; Valenti, G.; Paolucci, F. Insights into the mechanism of coreactant electrochemiluminescence facilitating enhanced bioanalytical performance. *Nat. Commun.* **2020**, *11*, 2668.

(19) Villani, E.; Inagi, S. Mapping the Distribution of Potential Gradient in Bipolar Electrochemical Systems through Luminol Electrochemiluminescence Imaging. *Anal. Chem.* **2021**, *93* (23), 8152-8160.

(20) Ma, C.; Wu, W.; Li, L.; Wu, S.; Zhang, J.; Chen, Z.; Zhu. J.-J. Dynamically imaging collision electrochemistry of single electrochemiluminescence nano-emitters. *Chem. Sci.* **2018**, *9* (29), 6167-6175.

(21) Valenti, G.; Fiorani, A.; Li, H.; Sojic, N.; Paolucci, F. Essential Role of Electrode Materials in Electrochemiluminescence Applications. *ChemElectroChem* **2016**, *3* (12), 1990-1997.

([22]) Yuan, Y.; Han, S.; Hu, L.; Parveen, S.; Xu, G. Coreactants of tris(2,2'-bipyridyl)ruthenium(II) Electrogenerated Chemiluminescence. *Electrochim. Acta* **2012**, *82*, 484-492.

([23]) Haghighatbin, M. A.; Laird, S. E.; Hogan, C. F. Electrochemiluminescence of cyclometalated iridium (III) complexes. *Curr. Opin. Electrochem.* **2018**, *7*, 216-223.

([24]) Kapturkiewicz, A. Cyclometalated iridium(III) chelates-a new exceptional class of the electrochemiluminescent luminophores. *Anal. Bioanal. Chem.* **2016**, *408* (25), 7013-7033.

([25]) Chen, L.; Hayne, D. J.; Doeven, E. H.; Agugiaro, J.; Wilson, D. J. D.; Henderson, L. C.; Connell, T. U.; Nai, Y. H.; Alexander, R.; Carrara, S.; Hogan, C. F.; Donnelly, P. S.; Francis, P. S. A conceptual framework for the development of iridium(III) complex-based electrogenerated chemiluminescence labels. *Chem. Sci.* **2019**, *10* (37), 8654-8667.

(26) Villani, E.; Valenti, G.; Marcaccio, M.; Mattarozzi, L.; Barison, S.; Garoli, D.; Cattarin, S.; Paolucci, F. Coreactant electrochemiluminescence at nanoporous gold electrodes. *Electrochim. Acta* **2018**, *277*, 168-175.

([27]) Fiorani, A.; Eßmann, V.; Santana Santos, C.; Schuhmann, W. Enhancing Electrogenerated Chemiluminescence on Platinum Electrodes through Surface Modification. *ChemElectroChem* **2020**, *7* (5), 1256-1260.

([28]) Zu, Y.; Bard, A. J. Electrogenerated Chemiluminescence. 66. The Role of Direct Coreactant Oxidation in the Ruthenium Tris(2,2')bipyridyl/Tripropylamine System and the Effect of Halide Ions on the Emission Intensity. *Anal. Chem.* **2000**, *72* (14), 3223-3232

(29) Parveen, S.; Chen, Y.; Yuan, Y.; Hu, L.; Zhang, W.; Gilani, M. R. H. S.; Shi, Y.; Aziz-ur-Rehman, Xu, G. Electrochemiluminescence of $[Ru(bpy)_3]^{2+}$/tripropylamine at glassy carbon, platinum, and palladium electrodes. *Sens. Actuators, Rep.* **2021**, DOI:10.1016/j.snr.2021.100062.

(30) https://www.mesoscale.com/en/technical_resources/our_technology/ecl (accessed 31st January, 2022).

(31) http://roche-html5.coservice.ch/app/webroot/book/en/ecl-unique-immunoassay-technology.html (accessed 31st January, 2022).

(32) Erler, K. Elecsys® immunoassay systems using electrochemiluminescence detection. *Wien. Klin. Wochenschr., Suppl.* **1998**, *110* (3), 5-10.

(33) Leland, J. K.; Powell, M. J. Electrogenerated Chemiluminescence: An Oxidative-Reduction Type ECL Reaction Sequence Using Tripropyl Amine. *J. Electrochem. Soc.* **1990**, *137* (10), 3127-3131.

(34) Rubinstein, I.; Bard, A. J. Electrogenerated chemiluminescence. 37. Aqueous ecl systems based on tris(2,2'-bipyridine)ruthenium(2+) and oxalate or organic acids. *J. Am. Chem. Soc.* **1981**, *103* (3), 512-516.

(35) White, H. S.; Bard, A. J. Electrogenerated chemiluminescence. 41. Electrogenerated chemiluminescence and chemiluminescence of the Ru(2,2'-bpy)$_3^{2+}$-$S_2O_8^{2-}$ system in acetonitrile-water solutions. *J. Am. Chem. Soc.* **1982**, *104* (25), 6891-6895.

(36) Kerr, E.; Doeven, E. H.; Wilson, D. J. D.; Hogan, C. F.; Francis, P. S. Considering the chemical energy requirements of the tri-*n*-propylamine co-reactant pathways for the judicious design of new electrogenerated chemiluminescence detection systems. *Analyst* **2016**, *141* (1), 62-69.

(37) Fiorani, A.; Irkham; Valenti, G.; Einaga, Y.; Paolucci F. Diamond Electrodes for Electrogenerated Chemiluminescence in *Nanocarbon Electrochemistry;* Yang, N., Zhao, G., Foord, J. S., Eds.; John Wiley and Sons Ltd, **2020**; pp 285-321.

(38) Fiorani, A.; Irkham; Valenti, G.; Paolucci, F.; Einaga, Y. Electrogenerated Chemiluminescence with Peroxydisulfate as a Coreactant Using Boron Doped Diamond Electrodes. *Anal. Chem.* **2018**, *90* (21), 12959-12963.

(39) Macpherson, J. V. A practical guide to using boron doped diamond in electrochemical research. *Phys. Chem. Chem. Phys.* **2015**, *17* (5), 2935-2949.

(40) Irkham; Watanabe, T.; Fiorani, A.; Valenti, G.; Paolucci, F.; Einaga, Y. Co-reactant-on-Demand ECL: Electrogenerated Chemiluminescence by the in Situ Production of $S_2O_8^{2-}$ at Boron-Doped Diamond Electrodes. *J. Am. Chem. Soc.* **2016**, *138* (48), 15636-15641.

(41) Irkham; Fiorani, A.; Valenti, G.; Kamoshida, N.; Paolucci, F.; Einaga, Y. Electrogenerated Chemiluminescence by in Situ Production of Coreactant Hydrogen Peroxide in Carbonate Aqueous Solution at a Boron-Doped Diamond Electrode. *J. Am. Chem. Soc.* **2020**, *142* (3), 1518-1525.

(42) Honda, K.; Yoshimura, M.; Rao, T. N.; Fujishima, A. Electrogenerated Chemiluminescence of the Ruthenium Tris(2,2')bipyridyl/Amines System on a Boron-Doped Diamond Electrode. *J. Phys. Chem. B* **2003**, *107* (7), 1653-1663.

(43) Honda, K.; Noda, T.; Yoshimura, M.; Nakagawa, K.; Fujishima, A. Microstructural Heterogeneity for Electrochemical Activity in Polycrystalline Diamond Thin Films Observed by Electrogenerated Chemiluminescence Imaging. *J. Phys. Chem. B* **2004**, *108* (41), 16117-16127.

(44) Yang, Y.; Oh, J.-W.; Kim, Y.-R.; Terashima, C.; Fujishima, A.; Kim, J. S.; Kim, H. Enhanced electrogenerated chemiluminescence of a ruthenium tris(2,2')bipyridyl/tripropylamine system on a boron-doped diamond nanograss array. *Chem. Commun.* **2010**, *46* (31), 5793-5795.

(45) Sentic, M.; Virgilio, F.; Zanut, A.; Manojlovic, D.; Arbault, S.; Tormen, M.; Sojic, N.; Ugo, P. Microscopic imaging and tuning of electrogenerated chemiluminescence with boron-doped diamond nanoelectrode arrays. *Anal. Bioanal. Chem.* **2016**, *408* (25), 7085-7094.

(46) Sakanoue, K.; Fiorani, A.; Irkham; Einaga, Y. Effect of Boron-Doping Level and Surface Termination in Diamond on Electrogenerated Chemiluminescence. *ACS Appl. Electron. Mater.* **2021**, *3* (9), 4180-4188.

(47) Irkham; Rais, R. R.; Ivandini, T. A.; Fiorani, A.; Einaga, Y. Electrogenerated Chemiluminescence of Luminol Mediated by Carbonate Electrochemical Oxidation at a Boron-Doped Diamond. *Anal. Chem.* **2021**, *93* (4), 2336-2341.

(48) Zoski, C. G. Handbook of Electrochemistry; Elsevier, **2007**.

(49) Egger, M.; Josel, H.; Gabriele, P. **2001**. Use of derivatized reagents in chemiluminescence and electrochemiluminescence detection methods. US patent 6281021, filled June 18, 1999.

(50) Zhou, X.; Zhu, D.; Liao, Y.; Liu, W. Liu, H.; Ma, Z.; Xing, D. Synthesis, labeling and bioanalytical applications of a tris(2,2'-bipyridyl)ruthenium(II)-based electrochemiluminescence probe. *Nat. Protoc.* **2014**, *9*, 1146-1159.

(51) Balmer, R. S.; Brandon, J. R.; Clewes, S. L.; Dhillon, H. K; Dodson, J. M.; Friel, I.; Inglis, P. N.; Madgwick, T. D.; Markham, M. L; Mollart, T. P.; Perkins, N.; Scarsbrook, G. A.; Twitchen, D. J.; Whitehead, A. J.; Wilman J. J.; Woollard, S. M. *J. Phys.: Condens. Matter* **2009**, *21* (36), 364221.

(52) Grushko, V.; Lübben, O.; Chaika, A. N.; Novikov, N.; Mitskevich, E.; Chepugov, A.; Lysenko, O.; Murphy, B. E.; Krasnikov S. A.; Shvets, I. V. Atomically resolved STM imaging with a diamond tip: simulation and experiment. *Nanotechnology* **2014**, *25* (2), 025706.

(53) Ogose, T.; Kasahara, S.; Ikemiya, N.; Hoshi, N.; Einaga, Y.; Nakamura. M. In Situ ATR-IR Observation of the Electrochemical Oxidation of a Polycrystalline Boron-Doped Diamond Electrode in Acidic Solutions. *J. Phys. Chem. C* **2018**, *122* (48), 27456-27461.

(54) Cobb, S. J.; Ayres, Z. J.; Newton, M. E.; Macpherson, J. V. Deconvoluting Surface-Bound Quinone Proton Coupled Electron Transfer in Unbuffered Solutions: Toward a Universal Voltammetric pH Electrode. *J. Am. Chem. Soc.* **2019**, *141* (2), 1035-1044.

(55) Kasahara, S.; Natsui, K.; Watanabe, T.; Yokota, Y.; Kim, Y.; Iizuka, S.; Tateyama, Y.; Einaga, Y. Surface Hydrogenation of Boron-Doped Diamond Electrodes by Cathodic Reduction. *Anal. Chem.* **2017**, *89* (21), 11341-11347.

(56) Kasahara, S.; Ogose, T.; Ikemiya, N.; Yamamoto, T.; Natsui, K.; Yokota, Y.; Wong, R. A.; Iizuka, S.; Hoshi, N.; Tateyama, Y.; Kim, Y.; Nakamura, M.; Einaga, Y. In Situ Spectroscopic Study on the Surface Hydroxylation of Diamond Electrodes. *Anal. Chem.* **2019**, *91* (8), 4980-4986.

(57) The term "onset potential" is used only to describe qualitatively the ECL peaks. See: Li, D.; Batchelor-McAuley, C.; Compton, R. G. Some thoughts about reporting the electrocatalytic performance of nanomaterials. *Appl. Mater. Today*, **2020**, *18*, 100404.

(58) Details on thermodynamic of Tris(2,2'-bipyridine)ruthenium(II)/TPrA system are available in the supporting information, paragraph 4.

(59) Kanoufi, F.; Zu, Y.; Bard, A. J. Homogeneous Oxidation of Trialkylamines by Metal Complexes and Its Impact on Electrogenerated Chemiluminescence in the Trialkylamine/Ru(bpy)$_3^{2+}$ System. *J. Phys. Chem. B* **2001**, *105* (1), 210-216.

(60) Thompson, D. W.; Ito, A.; Meyer, T. J. [Ru(bpy)$_3$]$^{2+*}$ and Other Remarkable Metal-to- Ligand Charge Transfer (MLCT) Excited States. *Pure Appl. Chem.* **2013**, *85* (7), 1257-1305.

(61) Miao, W.; Choi, J.; Bard, A. J. Electrogenerated Chemiluminescence. 69: The Tris(2,2'-bipyridine)ruthenium(II), (Ru(bpy)$_3^{2+}$)/Tri-*n*-propylamine (TPrA) System Revisited-A New Route Involving TPrA$^{\cdot+}$ Cation Radicals. *J.Am. Chem. Soc*. **2002**, *124* (48), 14478-14485.

(62) Sentic, M.; Milutinovic, M.; Kanoufi, F.; Manojlovic, D.; Arbault, S.; Sojic, N. Mapping electrogenerated chemiluminescence reactivity in space: mechanistic insight into model systems used in immunoassays. *Chem. Sci.* **2014**, *5* (6), 2568-2572.

(63) Yamaguchi, C.; Natsui, K.; Iizuka, S.; Tateyama, Y.; Einaga, Y. Electrochemical properties of fluorinated boron-doped diamond electrodes via fluorine-containing plasma treatment. *Phys. Chem. Chem. Phys.* **2019**, *21* (25), 13788-13794.

(64) Zu, Y.; Bard, A. J. Electrogenerated Chemiluminescence. 67. Dependence of Light Emission of the Tris(2,2')bipyridylruthenium(II)/Tripropylamine System on Electrode Surface Hydrophobicity. *Anal. Chem.* **2001**, *73* (16), 3960-3964.

(65)Valenti, G.; Zangheri, M.; Sansaloni, S. E.; Mirasoli, M.; Penicaud, A.; Roda, A.; Paolucci, F. Transparent Carbon Nanotube Network for Efficient Electrochemiluminescence Devices. *Chem. Eur. J.* **2015**, *21* (36), 12640-12645.

(66) McLntire, G. L.; Dorsey, J. G. Micelles in Analytical Chemistry. *Crit. Rev. Anal. Chem.* **1990**, *21* (4), 257-278.

(67) Rusling, J. F. Electrochemistry in micelles and microemulsions. In *Encyclopedia of Electrochemistry*; Wiley-VCH, **2007**.

(68) Mukerjee, P.; Mysels, K. J. *Critical Micelle Concentrations of aqueous surfactant systems*; US Department of Commerce, National Bureau of Standards: Washington, D.C., **1971**.

(69) Xu, G.; Pang, H.; Xu, B.; Dong, S.; Wong, K. Enhancing the electrochemiluminescence of tris(2,2'-bipyridyl)ruthenium(II) by ionic surfactants. *Analyst*. **2005**, *130* (4), 541-544

(70) Li, F.; Zu, Y. Effect of Nonionic Fluorosurfactant on the Electrogenerated Chemiluminescence of the Tris(2,2'-bipyridine)ruthenium(II)/Tri-*n*-propylamine System: Lower Oxidation Potential and Higher Emission Intensity. *Anal. Chem.* **2004**, *76* (6), 1768-1772

(71) Ouyang, J.; Bard, A. J. Electrogenerated Chemiluminescence. 50. Electrochemistry and Electrogenerated Chemiluminescence of Micelle Solubilized $Os(bpy)_3^{2+}$. *Bull. Chem. Soc. Jpn.* **1988**, *61* (1), 17-24.

(72) Naidu, K. T.; Prabhu, N. P. Protein Surfactant Interaction: Sodium Dodecyl Sulfate-Induced Unfolding of Ribonuclease A. *J. Phys. Chem. B* **2011**, *115* (49), 14760–14767.

(73) Waner, M. J.; Navrotskaya, I.; Bain, A.; Oldham, E. D.; Mascotti, D. P. Thermal and Sodium Dodecylsulfate Induced Transitions of Streptavidin. Biophys. J. **2004**, *87* (4), 2701-2713.

(74) Daviddi, E.; Oleinick, A.; Svir, I.; Valenti, G.; Paolucci, F.; Amatore, C. Theory and Simulation for Optimising Electrogenerated Chemiluminescence from Tris(2,2'-bipyridine)-ruthenium(II)-Doped Silica Nanoparticles and Tripropylamine. *ChemElectroChem* **2017**, *4* (7), 1719 -1730.

(75) Fiorani, A.; Han, D.; Jiang, D.; Fang, D.; Paolucci, F.; Sojic, N.; Valenti, G. Spatially resolved electrochemiluminescence through a chemical lens. *Chem. Sci.* **2020**, *11* (38), 10496-10500.

(76) Kalyanasundaram, K. Photophysics, photochemistry and solar energy conversion with tris(bipyridyl)ruthenium(II) and its analogues. *Coord. Chem. Rev.* **1982**, *46*, 159-244.

(77) Delaive, P. J.; Foreman, T. K.; Giannotti, C.; Whitten, D. G. Photoinduced Electron Transfer Reactions of Transition-Metal Complexes with Amines. Mechanistic Studies of Alternate Pathways to Back Electron Transfer. *J. Am. Chem. Soc*. **1980**, *102* (17), 5627-5631.

(78) Chen, Z.; Zu, Y. Electrogenerated Chemiluminescence of the Tris(2,2'-bipyridine)ruthenium(II)/Tri-n-propylamine (TPrA) System: Crucial Role of the Long Lifetime of $TPrA^{\bullet+}$ Cation Radicals Suggested by Electrode Surface Effects. *J. Phys. Chem. C* **2008**, *112* (42), 16663-16667.

(79) Adsetts, J. R.; Chu, K.; Hesari, M.; Ma, J.; Ding, Z. Absolute Electrochemiluminescence Efficiency Quantification Strategy Exemplified with $Ru(bpy)_3^{2+}$ in the Annihilation Pathway. *Anal. Chem.* **2021**, *93* (33), 11626-11633.

(80) Chu, K.; Adsetts, J. R.; Ma, J.; Zhang, C.; Hesari, M.; Yang, L.; Ding, Z. Physical Strategy to Determine Absolute Electrochemiluminescence Quantum Efficiencies of Coreactant Systems Using a Photon-Counting Photomultiplier Device. *J. Phys. Chem. C* **2021**, *125* (40), 22274-22282.

(81) Fernandez-Hernandez, J. M.; Longhi, E.; Cysewski, R.; Polo, F.; Josel, H.-P.; De Cola, L. Photophysics and Electrochemiluminescence of Bright Cyclometalated Ir(III) Complexes in Aqueous Solutions. *Anal. Chem.* **2016**, *88* (8), 4174-4178

(82) Yu, L.; Liu, Y.; Zhou, M. Improved electrochemiluminescence labels for heterogeneous microbead immunoassay. *Anal. Bioanal. Chem.* **2016**, *408* (25), 7095-7103.

(83) Factor, B.; Muegge, B.; Workman, S.; Bolton, E.; Bos, J.; Richter, M. M. Surfactant Chain Length Effects on the Light Emission of Tris(2,2'-bipyridyl)ruthenium(II)/Tripropylamine Electrogenerated Chemiluminescence. *Anal. Chem*. **2001**, *73* (19), 4621-4624.

(84) Albrecht, W. N.; Stephenson, R. L. Health hazards of tertiary amine catalysts. S*cand. J. Work Environ. Health* **1988**, *14* (4), 209-219.

(85) Kerr, E.; Alexander, R.; Francis, P. S.; Guijt, R. M.; Barbante, G. J.; Doeven, E. H. A Comparison of Commercially Available Screen-Printed Electrodes for Electrogenerated Chemiluminescence Applications. *Front. Chem.* **2021**, *8*, 628483.

(86) Muzyka, K.; Sun, J.; Fereja, T. H.; Lan, Y.; Zhang, W.; Xu, G. Boron-doped diamond: current progress and challenges in view of electroanalytical applications. *Anal. Methods* **2019**, *11* (4), 397-414.

For TOC only

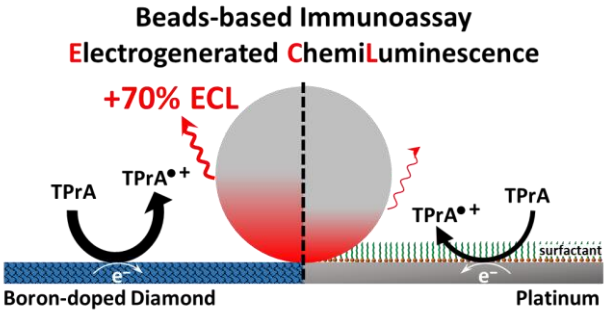

This research investigated the electrochemiluminescence of $Ru(bpy)_3^{2+}$/tri-*n*-propylamine system on boron-doped diamond electrodes where the $Ru(bpy)_3^{2+}$ is bound on microbeads mimicking an electrochemiluminescence immunoassay. By boron-doped diamond electrode the ECL intensity is 70% higher that platinum electrode which is currently used in clinical